Measurement 208 (2023) 112469

Contents lists available at ScienceDirect

Measurement

journal homepage: www.elsevier.com/locate/measurement

Uncertainty budget of a large-range nanopositioning platform based on Monte Carlo simulation

L.C. Díaz-Pérez [a,*], M. Torralba [b], L. Muro [a], J.A. Albajez [a], J.A. Yagüe-Fabra [a]

[a] I3A, Universidad de Zaragoza, Zaragoza, Spain
[b] Centro Universitario de la Defensa, Zaragoza, Spain

ARTICLE INFO

Keywords:
Nano-positioning
Measuring uncertainty
Uncertainty budget
Monte Carlo

ABSTRACT

The objective of precision systems design is to obtain machines with very high and totally predictable work-zone accuracies. In already functional systems, where the errors can be measured, this is achieved by error correction and compensation. The aim of this work is to propose an uncertainty budget methodology to obtain the final measuring uncertainty of precise measuring systems, after error compensation. The case study is a nano-positioning platform, referred as NanoPla, with a confocal sensor integrated as measuring instrument. The NanoPla performs precise positioning in a large range of 50 mm × 50 mm, and its target is surface topography characterization, at a submicrometre scale. After performing the uncertainty budget of the NanoPla, Monte Carlo method is used to obtain the final measuring uncertainty along the whole NanoPla working range, considering all the casuistry. By studying the results, the authors are able to propose solutions to minimize the final measuring uncertainty.

1. Introduction

The used of precise and miniaturized components and mechanisms in varied fields such as electronics, renewable energies and even astronomy has increased in the last decades [1]. This has resulted in the growing prominence of the precision systems required to manufacture and control these components. Precision systems design principles are crucial since they require geometric accuracy in the submicrometre scale and, consequently, they have been subject of many researches over the years [2–6].

According to Mckeown [2], the objective of precision systems design is to have machines with very high, totally predictable work-zone accuracies. Similarly, Leach and Smith coincide on the fact that the objective is to create a process for which the outcomes are deterministic and controllable over a range of operations, with unpredictable deviations from a desired result being as small as is physically and economically possible [7]. Already in 1986, McKeown outlined "eleven principles and techniques" of precision machine design [5]. These principles have been later reviewed and updated by authors like Schellekens [6,8]. More recent researches focus on the scalability of these precision design principles for precision systems of various working ranges [9].

One of these principles is error budgeting, which is defined by Hale in [4] as "an important deterministic tool that provides a systematic way to predict and/or control the repeatable and no repeatable errors of a machine". The error budget of a precision system analyses all relevant error influences, and allows calculating the uncertainty and identifying its main contributors [10]. Reducing and avoiding error sources, correcting repeatable errors and compensating known errors results in achieving an accurate system. Therefore, once the main contributors are identified, pertinent changes in the design must be considered to minimize their effect. In [9], four mitigation strategies are identified: error avoidance, error reduction, error correction and error compensation. Error avoidance and reduction techniques are applied during the early stages of the design phase and, hence, some error values need to be estimated. On the other hand, error correction and compensation are applied to an already functional system, where the errors can be measured, directly or indirectly.

There has been extensive investigation into error modeling in precision machines [11–14]. In most of the reviewed literature, error budget methodology is applied during the design phase. For instance, the work presented in [15] utilizes the error budget methodology during the design of a piezo-micropositioner to minimize the effects of the geometric tolerance, material variation, and hysteresis errors. The error

* Corresponding author.
E-mail address: lcdiaz@unizar.es (L.C. Díaz-Pérez).

https://doi.org/10.1016/j.measurement.2023.112469
Received 10 August 2022; Received in revised form 15 November 2022; Accepted 9 January 2023
Available online 11 January 2023

budget methodology can also be used during the control system design, as it was done in [16] where Slocum's homogeneous transformation matrices [17] were used. Similarly, in [18], error budgeting is used to evaluate the main sources of the critical dimension in optical lithography. In [18], Monte Carlo simulations are used to estimate the contributions of the future tools and mask critical dimension errors. Another example is presented in [19], where the error sources of portable machines are analyzed by defining a mixed virtual-experimental model that quantifies the errors. The used methodology allows knowing the effect of different errors in a virtual model, before a real prototype is built. In [20], the error budget methodology is applied to analyze spatial frequency domain errors, to do so, apart from static errors, dynamic errors are also considered.

However, in the literature, it is hard to find error budget analyses performed on functional systems, where errors are identified by experiments performed directly in the system. A study of these characteristics is presented in [21], in which an error budget is perform in a micro-milling machine (ULPRE II^{TM}), using the method outlined in Slocum [17,4] and Walter et al. [22,23], including all the elements that affect the final accuracy of the micro-workpiece [24]. Another error budget performed in a functional machine is presented in [25], where the measurement uncertainty in an H-drive stage during high acceleration is evaluated. In that work, the errors are identified by experiments and finite element analysis. Monte Carlo method is used to simulate that all errors occur at the same time or place in the given direction. This method has been proven to be an advantageous technique when working with complex mathematical error models [18,25–28].

In the work here presented, the precision system subject of study is a nanopositioning platform, referred hereafter as NanoPla. The NanoPla is capable of performing precise positioning with a submicrometre accuracy in a large range of 50 mm × 50 mm [29]. The NanoPla has been designed at the University of Zaragoza and the first prototype is intended for the metrological characterization of large surfaces. The measuring instrument is attached to the moving platform that performs the large displacement. In particular, the main application of this first prototype will be surface topography characterization at nanometer scale of samples with relatively big planar areas, using an atomic force microscope (AFM) [17]. During the design phase, the measurement accuracy of the NanoPla was optimized using the error budget methodology [30]. This analysis allowed to estimate the maximum measurement error vector of the developed system before it was manufactured and assembled. At present, the first NanoPla prototype is completely functional. In this initial approach, due to the fragility of the AFM, a confocal sensor has been integrated in the NanoPla as measuring instrument.

The aim of this work is to propose an uncertainty budget methodology to obtain the final measuring uncertainty of precise measuring systems, after error compensation. This methodology is implemented in the NanoPla, by performing an assessment of all the errors that affect the final measurement. Systematic errors are compensated, and, in those cases, only the uncertainty of that compensation is taken into account. For this reason, in this work the error budget is referred as uncertainty budget. Monte Carlo simulations have been used to evaluate the uncertainty contribution of each identified error, as it was done in some of the reviewed literature (e.g. in [18,25]). Assessing the NanoPla uncertainty budget will allow to know the capacity of the NanoPla system to perform the metrological characterization of surfaces along its working range, to estimate the limits of the system performance, and to minimize, when possible, the main uncertainty sources. In addition, it will help to improve the design of future prototypes.

The remaining of this article is organized as follows: First, the NanoPla system is introduced, explaining its structure and main parts, and describing its measuring procedure. Then, the uncertainty budget is performed, for that purpose, first, the mathematical error model of the NanoPla is obtained, defining its transformation matrices and vectors. Once, all the uncertainty contributors are identified and located in the mathematical error model, Monte Carlo simulations are performed to propagate the uncertainties and to obtain the final measuring uncertainty of the NanoPla. The simulations are performed for different positions along the NanoPla working range, considering all the casuistry. Finally, the authors propose solutions to minimize the final measuring uncertainty, and conclusions are withdrawn from the results.

2. NanoPla overview

High precision positioning in a submicrometre range is an essential technology for applications such as surface characterization with scanning probe microscopes, and micro manufacturing. The demand for positioning systems capable of providing accurate positioning (nanometre resolution) in a large working range (from 10 mm up to 100 mm) has increased [31]. In this line of research, the NanoPla with a large range of 50 mm × 50 mm and submicrometre accuracy has been developed, manufactured and assembled. Its first prototype is intended for metrological applications, although it could be adapted for micro manufacturing processes, such as lithography. This section first describes the NanoPla structure and its components, and, then, the measuring procedure of the NanoPla system.

2.1. Nanopla structure and components

An exploded view of the NanoPla and a picture are shown in Fig. 1. It consists of three main layers: a fixed inferior base, a moving platform and a fixed superior base. In addition, the metrology frame of the NanoPla has two parts: metrology frame (I) and metrology frame (II). The metrology frame (I) is fixed to the moving platform while the metrology frame (II) is fixed to the inferior base. The moving platform is levitated by three airbearings and performs frictionless planar motion along the whole working range of 50 mm × 50 mm propelled by four linear motors. The XY-position of the platform is measured by a 2D laser interferometer system from Renishaw®, whereas out-of-plane spurious motions are measured by capacitive sensors from Lion Precision®. In the initial design of the NanoPla, it was contemplated that the metrology frame was made of Zerodur, which has a very low thermal expansion coefficient. However, due to the fragility and cost of the Zerodur, in the first prototype, the metrology frame has been made of aluminum alloy 7075-T6.

The NanoPla implements a two-stage architecture, having a commercial piezostage (model NPXY100Z10A from nPoint®) attached to the metrology frame of the inferior base to perform fine motion in a range of 100 μm × 100 μm in the XY-plane and of 10 μm in Z-axis, while the moving platform performs the coarse motion, positioning the instrument along the large working range. In metrological applications, the measuring instrument is attached to the moving platform, while the sample is placed at the sample holder of the commercial piezo stage.

The NanoPla actuators are four Halbach linear motors which were custom-made by the University of North Carolina at Charlotte. They consist of a three-phase stator and a magnet array. The stators are fixed to the superior base, while the magnet arrays, that are wireless, are fixed to the moving platform. The motors are placed symmetrically in parallel pairs, in a way that each pair provides motion in X and Y-axes respectively. Thus, the motion is planar, frictionless and without backlash.

The 2D laser system measures the position of the moving platform at each moment. It consists of the combination of three plane mirror laser interferometers. The system belongs to the Renishaw RLE10 laser interferometer family. Apart from two laser units (RLU); three sensor heads (RLD) and two plane mirrors (one per axis), an environmental control unit (RCU) and three interpolators (REE) have been acquired. One laser beam is aligned to the X-axis and the other two beams, to the Y-axis, sharing plane mirror. Having plane mirrors as reflectors allows to measure the plane motion [32]. In addition, apart from measuring motion in X and Y-axes, the laser system also measures the rotation around Z-axis, θ_z. The three laser heads are placed on the metrology frame (II) fixed to the inferior base, as shown in Fig. 2. The plane mirrors

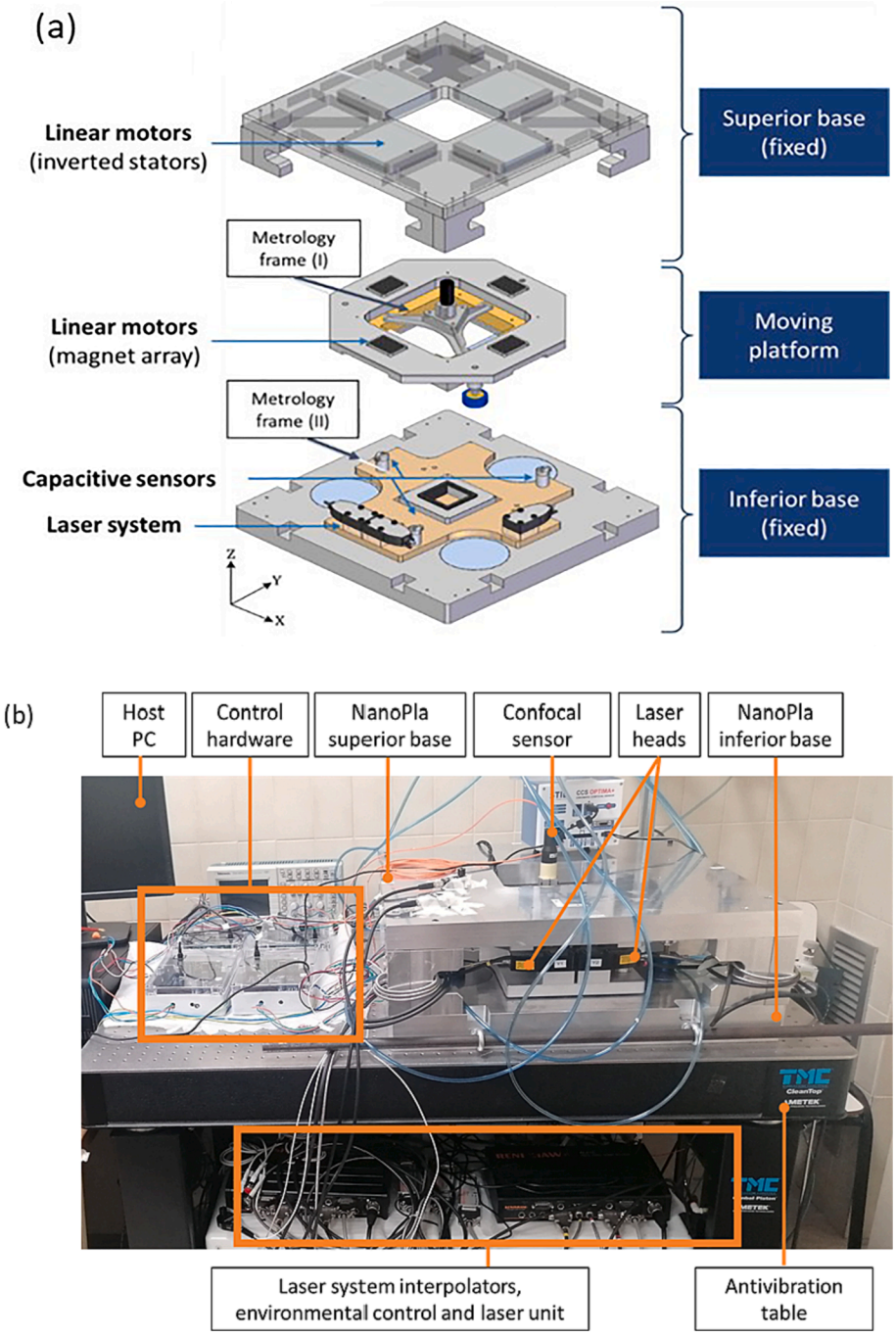

Fig. 1. (**a**) Exploded view of the NanoPla and (**b**) picture of the real setup.

are attached to the metrology frame (I) of the moving platform.

On the other hand, capacitive sensors are used to measure and compensate parasite out-of-plane motions. The capacitive sensor probes are placed at the metrology frame (II) of the inferior base (see Fig. 1), while the target surface is placed at the bottom of the moving platform. The three probes are separated approximately 120°. Small differences in the separation angle are a consequence of the lack of available space. The capacitive probes are the model C5-E from Lion Precision.

The measuring instrument is fixed to the metrology frame of the moving platform through a bracket (Fig. 3). This bracket consists of two parts: the first part is a holder screwed to the metrology frame, and the second part, which fastens the measuring instrument, is attached to the first one by a kinematic coupling preloaded by magnets. The second part is an adapter specific for each instrument and allows an easy integration of different measuring systems. The metrological instrument that has been used in this study is a chromatic confocal sensor. Specifically, the confocal sensor is the model CL4 with the magnifier MG 35 and the controller CCS Optima Plus from Stil®. The confocal sensor performs a 1D measurement without contact with the target, in a range of 4000 μm.

The piezostage is attached to the metrology frame through a levelling system consisting of three micrometres (Fig. 4). The micrometres are fixed to the metrology frame, while the piezostage lays on their spherical tips by means of a kinematic coupling of spheres and cylinders, preloaded by magnets. The measuring sample lays on the piezostage, which can be levelled by adjusting the micrometres. Two of the micrometres are manual (model DM-13L from Newport®), and one of them is motorized (model M−230.10 from Physik Instrumente®). The two manual micrometres have been adjusted during the assembly of the

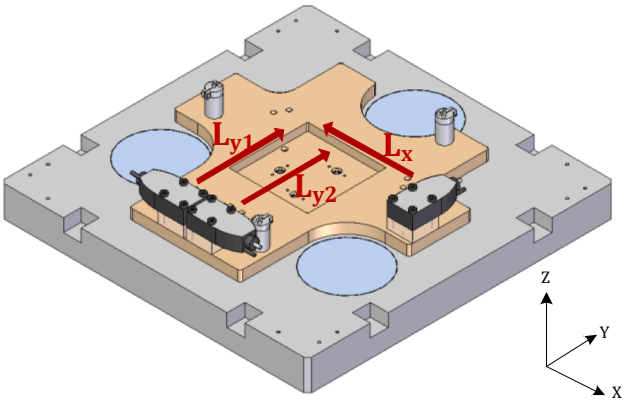

Fig. 2. Laser beam representation of the 2D laser system of the NanoPla inferior base.

levelling system in the NanoPla, and only the motorized micrometre is used for the fine tuning. The piezostage is levelled prior to the measuring procedure only if it is required to keep the measuring surface within the working range of the measuring instrument in Z-axis. Consequently, during the measuring procedure, the levelling system is considered static.

2.2. Nanopla measuring procedure

Before identifying the error sources, it is necessary to understand the NanoPla measuring procedure: First, the sample to be measured is placed at the sample holder of the piezostage (see Fig. 4). The confocal sensor position in Z-axis needs to be adjusted in order to have the sample surface contained inside its measuring range. If necessary, the piezostage can be levelled by adjusting the motorized micrometer of the levelling system Then, the measurement procedure is carried out in two well-differentiated processes that occur consecutively:

1. Positioning process: During the positioning process, the confocal sensor is positioned in XY-coordinates over the area of the sample that is going to be measured. The confocal sensor is fixed to the moving platform, whose movement in the XY-plane is performed by the NanoPla position control system. During the displacement, the moving platform is levitated by three airbearings. The control system performs the positioning of the moving platform in X and Y-axes, along the working range of 50 mm × 50 mm. The deviations in Z-axis position are caused by spurious motions, and they are not controlled, only monitored by the three capacitive sensors. Once the moving platform achieves the target position, the airbearings are shut down, the moving platform stops levitating, and the actuators are turned off. Finally, the moving platform and the confocal sensor remain static over the area of the sample to be measured.
2. Scanning process: The moving platform position in Z-axis is measured by the capacitive sensors, so that any deviation can be corrected in the final measurement. It is worth noting that the confocal sensor readouts are one-dimensional in Z-axis, consequently, in order to measure a XY-area, it is necessary to generate a scanning motion between sample and sensor. In this case, the scanning motion is provided by the commercial piezostage along the area of 100 μm × 100 μm in the XY-plane.

The final output of the system is a three-coordinate measurement, and it is calculated as follows:

- XY-coordinates: They represent the relative position between the confocal sensor axis and the sample. They are calculated as the composition of the displacement of the confocal sensor performed during the positioning process, provided by the moving platform; and the displacement of the sample performed during the scanning process, provided by the piezostage.
- Z-coordinate: The Z-coordinate is provided by the confocal sensor readout at the respective XY coordinates. The spurious motions of the confocal sensor in Z-axis are measured by the capacitive sensors and must be compensated in the readouts.

3. Uncertainty budget

The uncertainty budget methodology is a deterministic tool that helps identify, classify and quantify the influence of the system errors on its desired output [9]. The uncertainty budget must include all the elements that affect the final measurement uncertainty of the sample surface.

In this section, first, the NanoPla mathematical error model is defined, and the transformation matrices between the reference systems of the elements are analyzed and simplified. Finally, the uncertainty

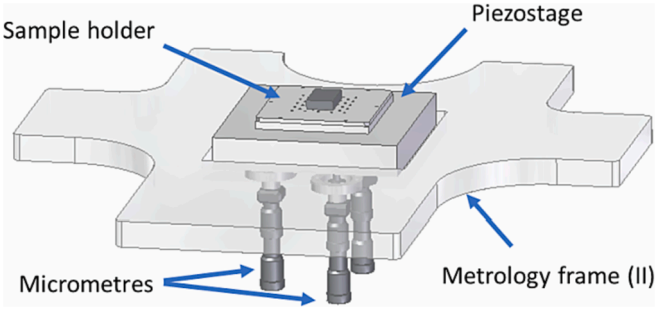

Fig. 4. Sample holder, piezostage, metrology frame (II) and levelling system.

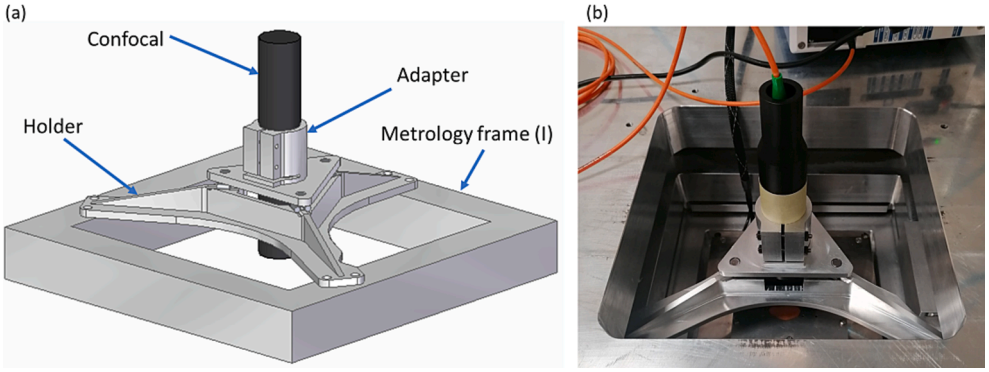

Fig. 3. (**a**) Measuring instrument attached to the metrology frame (I) and (**b**) picture of the real setup.

sources that affect the measuring process are identified, classified and quantified. It is important to note that, for the correct application of Monte Carlo method, apart from identifying all uncertainty sources, it is also required to identify their probability distribution.

3.1. Mathematical error model

In contrast to classic mathematical error models in which linear movements of the three axes are superposed [33], the NanoPla implements a two-stage motion, that combines the coarse planar motion of the moving platform (long range) and the fine translation in X,Y and Z-axes of the piezostage (short range).

Fig. 5 shows the global scheme of the measurement loop of the NanoPla, which involves metrology frame (I) and metrology frame (II). There are two kinematic chains that start at the fixed base {0}. The second element of the upper chain is the moving platform {1} that performs the coarse motion (50 mm × 50 mm) in the XY-plane. The measuring instrument, a confocal sensor in this case {CS}, is fixed to the moving platform through the bracket. The second element of the lower chain is the levelling system and the piezostage {LS} that are considered as an ensemble since they are attached together by a kinematic coupling. The piezostage provides the XYZ-fine motion (100 μm × 100 μm × 10 μm) to the sample {Sp} that is placed on its sample holder. The end of both chains is the point where the confocal sensor beam P_{CS} (0, 0, z_{CS}) intersects with the surface of the sample P_{Sp} (x_{sp}, y_{sp}, z_{sp}).

In the upper chain, the following relations between systems are considered:

$$P_1 = R_1^{CS} \cdot P_{CS} + T_1^{CS} \tag{1}$$

$$P_0 = R_0^1 \cdot P_1 + T_0^1 \tag{2}$$

Similarly, in the lower chain, the following relations between systems are considered:

$$P_{LS} = R_{LS}^{Sp} \cdot P_{Sp} + T_{LS}^{Sp} \tag{3}$$

$$P_0 = R_0^{LS} \cdot P_{LS} + T_0^{LS} \tag{4}$$

Where P_i is the point analyzed represented according to the {i} system, R_i^j is the rotation matrix from {i} to {j} systems; and T_i^j is the translation vector between {i} and {j} origins. Considering that P_{CS} and P_{Sp} are coincident, they can be expressed in the common coordinate reference system {0}, and the continuity Equation (6) can be obtained:

$$P_{Sp} = \left[R_{LS}^{Sp}\right]^{-1} \cdot \left[\left[R_0^{LS}\right]^{-1} \cdot \left[R_0^1 \cdot \left(R_1^{CS} \cdot P_{SC} + T_1^{CS}\right) + T_0^1 - T_0^{LS}\right] - T_{LS}^{Sp}\right] \tag{5}$$

In Equation (6), the transformation matrices and vectors define the connectivity relationship between elements. Introducing the uncertainties or known errors of the translations and rotations allows to study their propagation through the system and how they affect the measuring process. Thus, the overall measuring uncertainty is reflected in P_{Sp} vector.

3.2. Definition of the transformation matrices and vectors

In this section, the translation vectors and rotation matrices between elements are defined and revised to locate the existing errors, and simplify the mathematical expression of the kinematic model when possible. A rigid body behavior is assumed, which was demonstrated in a previous work after a finite element analysis verification in [29]. In addition, angular deviations are assumed to be small angles to simplify the rotation matrices. Moreover, the uncertainty budget focuses on the uncertainty propagation of the angular deviations, not the angular deviations per se. A sensitivity analysis has been performed taking into account the actual ranges of the angular errors' uncertainties (not higher than 5×10^{-5} rad), and it has been verified that the error introduced by these simplifications is negligible (<1nm). For simplification of the equation, the offsets between origins are considered inside the translation vectors.

- Transformation between coordinate reference system of the fixed base and coordinate reference system of the moving platform ({0}-{1}):
- Definition of axes and origin of coordinates: In the fixed base, the X-axis is defined by the laser system X-axis beam, while the Y-axis is orthogonal to it and contained in the XY plane formed by the beams. Similarly, in the moving platform, the X-axis is defined by the normal vector of the plane mirror of the X-axis laser beam. The origin of both coordinate systems is coincident when the moving platform is at the reference position ($x^{\{1\}} = 0$, $y^{\{1\}}$=0). The origin is contained in the plane formed by the beams of the laser system, at the reference position.
- Translation vector: The long-range motion of the moving platform in X and Y-axes ($x^{\{1\}}, y^{\{1\}}$) is contained in the translation vector. The vector also includes the linear motion errors in X, Y and Z-axes ($\delta_x^{\{1\}}$, $\delta_y^{\{1\}}, \delta_z^{\{1\}}$), and the lack of squareness between axes ($\alpha_{yx}^{\{1\}}, \alpha_{zx}^{\{1\}}, \alpha_{zy}^{\{1\}}$).

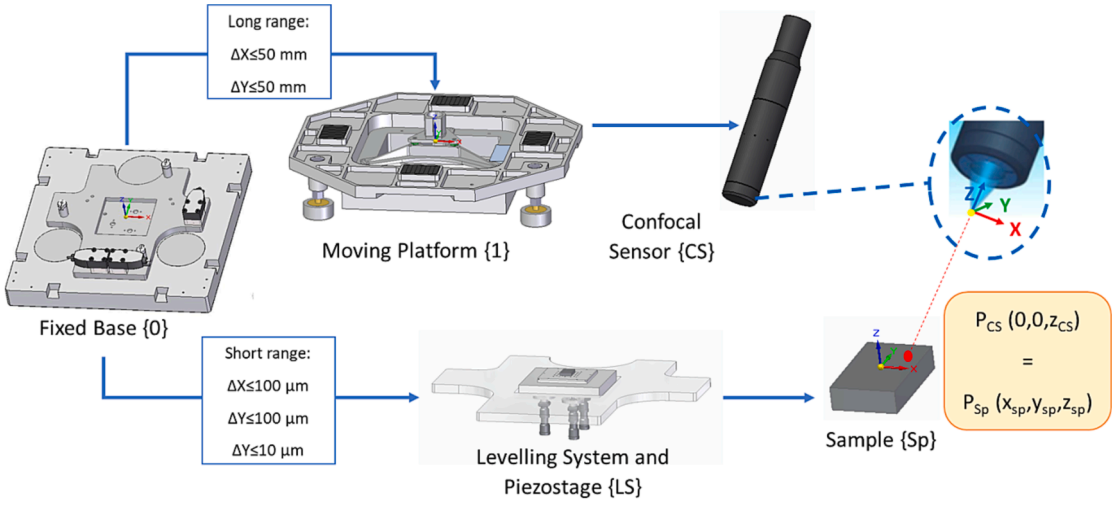

Fig. 5. Schematization of the complete measurement loop of the NanoPla stage.

$$T_0^1 = \begin{pmatrix} x^{\{1\}} + \delta_x^{\{1\}} \\ y^{\{1\}} + \delta_y^{\{1\}} - x^{\{1\}} \cdot \alpha_{yx}^{\{1\}} \\ \delta_z^{\{1\}} - x^{\{1\}} \cdot \alpha_{zx}^{\{1\}} - y^{\{1\}} \cdot \alpha_{zy}^{\{1\}} \end{pmatrix} \tag{6}$$

- Rotation matrix: Ideally, the moving platform is aligned with the fixed base and performs only linear displacement. However, there may be misalignments in the assembly and spurious rotations when performing motion ($\varepsilon_x^{\{1\}}, \varepsilon_y^{\{1\}} \varepsilon_z^{\{1\}}$).

$$R_0^1 = \begin{pmatrix} 1 & -\varepsilon_z^{\{1\}} & \varepsilon_y^{\{1\}} \\ \varepsilon_z^{\{1\}} & 1 & -\varepsilon_x^{\{1\}} \\ -\varepsilon_y^{\{1\}} & \varepsilon_x^{\{1\}} & 1 \end{pmatrix} \tag{7}$$

- Transformation between coordinate reference system of the moving platform and the coordinate reference system of the confocal sensor ({1}-{CS}). The confocal sensor is attached to the moving platform, thus, there is no relative motion. Therefore, the translation vector only considers the offset:
- Definition of axes and origin of coordinates: The Z-axis of the confocal sensor coordinate system is aligned with its beam. The origin of the coordinate system of the confocal sensor is the point along its working range at which the sensor readout is taken as the reference. If this point is not contained in the XY-plane of the moving platform reference system, there is an offset in Z-axis between the origins of both coordinate systems that must be considered (z_o^{CS}). It is worth noting that the position of the sensor can be adjusted depending on the sample height, so that the sample surface is contained within the sensor's working range. Therefore, this offset may be different for the measurement of each sample.

$$T_1^{CS} = \begin{pmatrix} 0 \\ 0 \\ z_o^{CS} \end{pmatrix} \tag{8}$$

- Rotation matrix: There may be some angular deviations between the Z-axes of both coordinate systems due to misalignments in the assembly. This rotation occurs during the assembly, before the measuring procedure, consequently, it is a rotation offset, i.e. its value is constant during the whole measuring procedure, independent on the position of the moving platform or the piezostage. Only the rotations around X and Y-axes are considered ($\varepsilon_{x,o}^{\{CS\}}$, $\varepsilon_{y,o}^{\{CS\}}$), since the rotation in Z-axis does not affect the measurement.

$$R_1^{CS} = \begin{pmatrix} 1 & 0 & \varepsilon_{y,o}^{CS} \\ 0 & 1 & -\varepsilon_{x,o}^{CS} \\ -\varepsilon_{y,o}^{CS} & \varepsilon_{x,o}^{CS} & 1 \end{pmatrix} \tag{9}$$

- Additionally, P_{CS} is the point where the confocal sensor beam intersects with the surface of the sample being measured, contained in the reference system of the confocal sensor ({CS}). It only has one component in Z-axis: Z_{CS}, and it can be obtained by extracting the measuring errors (ε_{CS}) to the readout provided by the sensor (z_{CS}^{exp}).

$$P_{CS} = \begin{pmatrix} 0 \\ 0 \\ Z_{CS} \end{pmatrix} = \begin{pmatrix} 0 \\ 0 \\ z_{CS}^{exp} - \varepsilon_{CS} \end{pmatrix} \tag{10}$$

- Transformation between coordinate reference system of the fixed base and coordinate reference system of the levelling system and piezostage ({0}-{LS}):
- Definition of axes and origin of coordinates: The X-axis of levelling system and piezostage reference system is defined along piezostage X-axis, while its Y-axis is contained in the plane defined by the surface of the sample holder. The origin of the reference system is considered at the center of the piezostage sample holder. Thus, there is an offset in the three axes between the origins of the reference system of the fixed base and of the levelling system and piezostage that must be considered in the translation vector ($x_o^{LS}, y_o^{LS}, z_o^{LS}$).
- Translation vector: The three micrometers of the levelling system are adjustable along their axes. However, this adjustment is done prior to the measuring procedure, therefore, the displacement is considered in the offset of the origin of coordinates instead of considering it as a translation. In addition, the sample holder of the piezostage is displaced in X, Y and Z-axes ($x^{\{S\}}, y^{\{S\}}, z^{\{S\}}$), performing the fine motion of the sample. The translation vector considers this translation plus the motion errors of the piezostage ($\delta_x^{\{S\}}$, $\delta_y^{\{S\}}$, $\delta_z^{\{S\}}$). The non-squareness error between axes of motion of the piezostage are considered negligible by its manufacturer, and, hence, not considered in the vector.

$$T_0^{LS} = \begin{pmatrix} x_o^{LS} + \left(x^{\{S\}} + \delta_x^{\{S\}}\right) \\ y_o^{LS} + \left(y^{\{S\}} + \delta_y^{\{S\}}\right) \\ z_o^{LS} + \left(z^{\{S\}} + \delta_z^{\{S\}}\right) \end{pmatrix} \tag{11}$$

- Rotation matrix: The XY plane of the levelling system rotates when the tip of the motorized micrometre moves along Z-axis. This rotation takes place before the measuring procedure; thus, it is a rotation offset ($\varepsilon_{x,o}^{LS}$, $\varepsilon_{y,o}^{LS}$, $\varepsilon_{z,o}^{LS}$). On the other hand, spurious rotations of the sample holder during the motion of the piezostage are considered negligible by its manufacturer. Consequently, they are not considered in this work.

$$R_0^{LS} = \begin{pmatrix} 1 & -\varepsilon_{z,o}^{LS} & \varepsilon_{y,o}^{LS} \\ \varepsilon_{z,o}^{LS} & 1 & -\varepsilon_{x,o}^{LS} \\ -\varepsilon_{y,o}^{LS} & \varepsilon_{x,o}^{LS} & 1 \end{pmatrix} \tag{12}$$

- Transformation between coordinate reference system of the levelling system and piezostage and the coordinate reference system of the sample ({LS}-{Sp}):
- Definition of axes and origin of coordinates: The reference system of the sample is defined by the workpiece itself. Therefore, there is an offset between both coordinate systems that must be considered. For simplicity, this offset (R_{LS}^{Sp}, T_{LS}^{Sp}) will be omitted.

Finally, Equation (5) can be reformulated by applying the simplifications that have been defined in this subsection:

$$P_{Sp} = \left[R_0^{LS}\right]^{-1} \cdot \left[R_0^1 \cdot \left(R_1^{CS} \cdot P_{CS} + T_1^{CS}\right) + T_0^1 - T_0^{LS}\right] \tag{14}$$

By decomposing the vector in the three axes, and eliminating the constant terms, Equation (15) is obtained for X-axis, and Equation 16 is obtained for Z-axis. The equation for Y-axis is omitted because it is symmetrical to X-axis. It is worth noting that the levelling system and piezostage offsets ($x_o^{LS}, y_o^{LS}, z_o^{LS}$) have been cancelled for being constant terms.

$$X_{P_s} = \left(x^{\{1\}} + \delta_x^{\{1\}}\right) - \left(x^{\{S\}} + \delta_x^{\{S\}}\right) + \left(z_{CS}^{exp} - \varepsilon_{CS}\right)\cdot\left(\left(\varepsilon_{y,o}^{CS} - \varepsilon_{y,o}^{LS}\right) + \varepsilon_z^{\{1\}}\cdot\left(\varepsilon_{x,o}^{CS} + \varepsilon_{y,o}^{CS}\cdot\varepsilon_{z,o}^{LS}\right) + \varepsilon_y^{\{1\}}\cdot\left(1 + \varepsilon_{y,o}^{CS}\cdot\varepsilon_{y,o}^{LS}\right) - \varepsilon_{x,o}^{CS}\cdot\varepsilon_{z,o}^{LS} + \varepsilon_x^{\{1\}}\cdot\left(\varepsilon_{x,o}^{CS}\cdot\varepsilon_{y,o}^{LS} - \varepsilon_{z,o}^{LS}\right)\right) + z_o^{CS}\cdot\left(\varepsilon_y^{\{1\}} - \varepsilon_x^{\{1\}}\cdot\varepsilon_{z,o}^{LS} - \varepsilon_{y,o}^{LS}\right) + \left(y^{\{1\}} + \delta_y^{\{1\}} - x^{\{1\}}\cdot\alpha_{yx}^{\{1\}} - y^{\{S\}} - \delta_y^{\{S\}}\right)\cdot\varepsilon_{z,o}^{LS} - \left(\delta_z^{\{1\}} - x^{\{1\}}\cdot\alpha_{zx}^{\{1\}} - y^{\{1\}}\cdot\alpha_{zy}^{\{1\}} - z^{\{S\}} - \delta_z^{\{S\}}\right)\cdot\varepsilon_{y,o}^{LS} \quad (15)$$

$$Z_{P_s} = \left(z_{CS}^{exp} - \varepsilon_{CS}\right) + \left(\delta_z^{\{1\}} - x^{\{1\}}\cdot\alpha_{zx}^{\{1\}} - y^{\{1\}}\cdot\alpha_{zy}^{\{1\}}\right) - \left(z^{\{S\}} + \delta_z^{\{S\}}\right) + \left(z_{CS}^{exp} - \varepsilon_{CS}\right)\cdot\left(\varepsilon_{y,o}^{CS}\cdot\varepsilon_{y,o}^{LS} + \varepsilon_{x,o}^{LS}\cdot\varepsilon_{x,o}^{CS} + \varepsilon_z^{\{1\}}\cdot\left(\varepsilon_{x,o}^{CS}\cdot\varepsilon_{y,o}^{LS} - \varepsilon_{y,o}^{CS}\cdot\varepsilon_{x,o}^{LS}\right) + \varepsilon_x^{\{1\}}\cdot\left(\varepsilon_{x,o}^{LS} - \varepsilon_{x,o}^{CS}\right) + \varepsilon_y^{\{1\}}\cdot\left(\varepsilon_{y,o}^{LS} - \varepsilon_{y,o}^{CS}\right)\right) + z_o^{CS}\cdot\left(\varepsilon_y^{\{1\}}\cdot\varepsilon_{y,o}^{LS} + \varepsilon_x^{\{1\}}\cdot\varepsilon_{x,o}^{LS}\right) + \left(x^{\{1\}} + \delta_x^{\{1\}} - x^{\{S\}} - \delta_x^{\{S\}}\right)\cdot\varepsilon_{y,o}^{LS} - \left(y^{\{1\}} + \delta_y^{\{1\}} - x^{\{1\}}\cdot\alpha_{yx}^{\{1\}} - y^{\{S\}} - \delta_y^{\{S\}}\right)\cdot\varepsilon_{x,o}^{LS} \quad (16)$$

3.3. Uncertainty contributors identification

After defining the mathematical error model and the transformation matrices of the NanoPla, this subsection proceeds to identify, classify and quantify the uncertainty contributors, to, at last, estimate their influence in the final output of the system. It is worth highlighting that systematic errors are compensated when possible, and, in those cases, only the uncertainty of that compensation is taken into account in the uncertainty budget.

The uncertainty budget contributors are commonly classified according to their source. In [30], the errors were classified into three groups: instrumental, alignment and environmental errors, as it was done in [34]. However, in this work, the sources are first classified in two main groups, depending on whether they affect the positioning process or the scanning process. In each group, the uncertainty sources are divided in three subgroups, respectively, depending on their source: system components inaccuracies, misalignments and environmental deviations. When possible, the errors have been experimentally measured, and the experimental data have been subject to statistical analysis in order to estimate their probability function. All the experimental measurements have been carried out in the metrology laboratory where the NanoPla is placed. The temperature variation in the laboratory was measured experimentally and it has a Weibull distribution with a standard deviation of 0.61 °C. The errors that cannot be measured, have been evaluated by other means, such as the calibration certificate of the manufacturer. In these cases, if the probability function is not stated, it is assumed to be uniform to consider the worst-case scenario.

3.3.1. Positioning process

The NanoPla positioning control system is in charge of performing the motion of the moving platform during the positioning process, its positioning uncertainty was estimated to be 0.5 μm [35]. This position uncertainty refers to the capacity of the control system to displace the moving platform to a target location, considering the positioning error of the control system as the difference between the achieved position and the target position, which could be caused, for instance, by the resolution of the control hardware of the motors. However, in this work, it is considered that during the scanning process, the moving platform remains static, not levitating. Thus, the final output of the positioning process is the XY position of the moving platform, provided by the laser system, despite of the control system errors which can be later corrected by the piezostage. Consequently, the control system errors are not considered in this analysis.

During the positioning process, the uncertainties are caused by the inaccuracies of the 2D laser system components, the misalignments of its assembly, and by the thermal expansion of the metrology frame:

a) System components inaccuracies:

- Inaccuracies of the 2D laser system ({0}-{1}): The laser system has three detector heads that provide three measurements, two in Y-axis and one in X-axis. The position in Y-axis is calculated as the average between the two measurements in Y-axis, and the rotation around Z-axis ($\varepsilon_z^{\{1\}}$) is calculated as the arctangent between the difference of the two measurements in Y-axis and the distance in X-axis between them.
  - Laser system wave instability: The laser system wavelength instability of the RLU10 laser unit is given by the manufacturer and it has a value of 50 ppb (1–8 h) in the displacement error. Considering the maximum displacement of the moving platform, that is 25 mm, it supposes an error of 1.25 nm ($\delta_x^{\{1\}}, \delta_y^{\{1\}}$).
  - Laser sensor resolution: The minimum output resolution that the RCU is able to achieve is 9.88 nm. This resolution is improved by the system interpolators (REE) to 1.58 nm ($\delta_x^{\{1\}}, \delta_y^{\{1\}}$). This value is given by the manufacturer, and it was also experimentally measured [36].
  - Laser beam mixing: Laser beam mixing or spurious beams lead to a non-linearity error lower than 2 nm ($\delta_x^{\{1\}}, \delta_y^{\{1\}}$) in the RLD detector head. This value is given by the manufacturer.
  - Root mean square deviation (RMSD) of the laser system readouts: It was measured experimentally in [36]. The standard deviations of the measurements recorded during 60 min were 5.4 nm for X- axis, and 4.13 nm and 4.2 nm for the two laser detectors of Y-axis, respectively. In this study, a RMSD of 5.4 nm with a normal distribution is going to be considered for the three detectors ($\delta_x^{\{1\}}, \delta_y^{\{1\}}$).

b) Misalignments:

- Plane mirror form errors ({0}-{1}): The non-uniform surface of the plane mirrors is characterized by their flatness. The lack of flatness results in a reading error of the laser system, whose value is given by the manufacturer of the reflector, and it is lower than λ/10 per 100 mm (where λ is the laser wavelength equal to 633 nm), with a uniform distribution. Despite of the different length of the mirrors, those errors are identical: 15.75 nm in X- and Y-axes ($\delta_x^{\{1\}}, \delta_y^{\{1\}}$).
- Laser system assembly ({0}-{1}): The laser heads are fixed to the metrology frame of the inferior base, while the plane mirrors are fixed to the metrology frame (I) of the moving platform. The assembly of the components inevitably leads to misalignments between laser beams and plane mirrors, and between these two and the plane of motion of the moving platform. These misalignments were addressed in a previous work [37] where it was calculated how they affect the final measurement of the system:
  - Misalignments between laser beam and plane mirror: The manufacturer defines a tight alignment tolerance between the laser beam and the normal vector of the plane mirror (1.2×10^{-4} rad). It applies to both pitch and yaw between laser beam and plane mirror. Considering 100 mm as the maximum possible distance between the mirror and the laser head in the setup, any deviations caused by the orthogonality error between the laser beam and plane are negligible ($\ll 1$ nm).
  - Misalignments between laser beams and plane of motion: As mentioned, the moving platform levitates over the fixed base, thus, the XY plane of motion is defined by the airbearing surfaces. Due to the fact that the motors are unguided, the laser beams projection in the plane of motion defines the axes of motion. Hence, in this case, there are no yaw errors. However, there is a pitch error (α_{pitch}) between each laser beam and the plane of motion which lead to linearity errors ($\delta_x^{\{1\}}, \delta_y^{\{1\}}$). The misalignments can be measured or obtained by calibration methods, and the errors compensated in the measurement. A self-calibration procedure was proposed in [37]. Therefore, only

the uncertainty with which the misalignments are obtained is going to be taken into account in this study, that is 25 nm, with a uniform distribution.

– Non-squareness between laser beams: The two laser beams in Y-axis are considered to be parallel since they are reflected in the same plane mirror. However, there is a non-squareness error between the laser beams in Y-axis and the laser beam in X-axis, $\alpha_{yx}^{\{1\}}$. The non-squareness error can be known by directly measuring the orthogonality between the two plane mirrors, or by calibration methods [37], and, then compensated. Thus, only the uncertainty with which the non-squareness is obtained is going to be taken into account in this study, that is 1×10^{-6} rad with a uniform distribution.

- Moving platform and inferior base assembly ({0}-{1}): The three airbearings of the moving platform displace over three surfaces fixed to the inferior base, keeping the air gap constant. As a consequence, the misalignments between the airbearing surfaces and the reference plane result in spurious motions that affect the position in Z-axis, measured by the capacitive sensors. Due to the fact that the measurements of the capacitive sensors are compensated from the confocal sensor readout, this error will be taken into account in the scanning process. However, it is worth noting that the angular deviations ($\varepsilon_x^{\{1\}}$, $\varepsilon_y^{\{1\}}$) are limited by the maximum angular deviations that the laser beams and the plane mirrors allow, that is 1.2×10^{-4} rad. It has been verified that in any case this limit is surpassed. Otherwise, the laser system would not work along the whole working range of the NanoPla.

c) Environmental deviations:

- Laser system refractive index environmental compensation ({0}-{1}): Environmental deviations in pressure, humidity and temperature result in refractive index variations, which are corrected in real time by the laser system environmental unit (RCU), which includes pressure and temperature sensors. The accuracy of the refractive index compensation is given by the manufacturer and it is 1 ppm. That means motion errors in the NanoPla XY-positioning ($\delta_x^{\{1\}}, \delta_y^{\{1\}}$) of 2.5 nm for $\Delta T = 1$ºC, with a uniform distribution.
- Thermal expansion of the metrology frame in the XY plane ({0}-{1}): The RCU of the laser system monitors the NanoPla temperature and allows compensating the thermal expansion that affects the measurement of the laser system. The error of that compensation was calculated experimentally, it follows a normal distribution with an average of 21 nm and a standard deviation of 19 nm for X-axis ($\delta_x^{\{1\}}$), and an average of 43 nm and a standard deviation of 24 nm for Y-axis ($\delta_y^{\{1\}}$). The compensation error averages are considered systematic errors and, thus, they are not taken into account in the uncertainty budget.

3.3.2. Scanning process

During the scanning process, the commercial piezostage provides the scanning motion to the sample. The confocal sensor remains completely static while measuring the distance to the sample in Z-axis. The spurious motions in Z-axis originated during the positioning process are measured by the capacitive sensors and compensated in the final measurement. Thus, during the scanning process, the uncertainties are caused by the inaccuracies of the piezostage, the confocal sensor, and the capacitive sensors, the misalignments of the assembly, and the thermal expansion of the components.

It is worth reminding that there is a relative motion between the moving platform and the fixed base, where the capacitive sensors and the piezostage are placed, thus, the spurious motions in Z-axis may be different for each position. In this subsection, the results at the reference position (0,0) are shown. However, the following section performs Monte Carlo simulations along the whole working range of the NanoPla.

a) System components inaccuracies:

- Capacitive sensors inaccuracies ({0}-{1}): There are three capacitive sensors (C1, C2, C3) that measure the spurious motion ($\delta_z^{\{1\}}$) of the moving platform in Z-axis, and, from their measurements, the angular deviations ($\varepsilon_x^{\{1\}}$, $\varepsilon_y^{\{1\}}$) of the moving platform can be inferred. The capacitive sensor probes are fixed to the metrology frame of the inferior base, while the capacitive targets are fixed to the moving platform. Although there are three sensor probes, the value compensated from the confocal readouts is the effective value at the center of the moving platform, that is coincident with the confocal sensor axis. The capacitive sensor inaccuracies are listed below:

  – Root Mean Square Deviations of the capacitive sensors' readouts: Each capacitive sensor readout has a RMSD, which depends on different factors, such as the quality of the target surface. The value of the RMSD of each of them has been experimentally measured in the NanoPla setup [38]. Its effective value at the centre of the moving platform is 34.18 nm ($\delta_z^{\{1\}}$), with a uniform distribution.

  – Capacitive sensors positioning error: Each capacitive sensor readout has a position error stated in its calibration certificate. Considering the worst case, the effective value at the centre of the moving platform is 60.80 nm ($\delta_z^{\{1\}}$).

- Confocal sensor inaccuracies ({CS}). It is worth highlighting that the NanoPla can integrate different types of measuring systems. In this work, the measuring instrument is a confocal sensor. Although, considering the capability of the NanoPla, the confocal sensor presents relatively high measuring errors, it has been selected as the measuring instrument in this first approach due to its simplicity. The confocal sensor performance has been characterized in a metrological measuring setup that has been designed and manufactured for the purpose, in order to isolate its errors from the ones of the NanoPla stage. The design of the metrological measuring setup minimizes the effects of thermal variations in the measuring distance. The correct performance of the confocal sensor has been verified by means of reference standards along its measuring range of 4,000 µm.
  - Confocal static noise: The manufacturer provides a measurement of the metrological characteristics of the instrument where specifies that the static noise at the center of the measuring range is 99 nm (ε_{CS}). Although in this work, this value is the one taken into account, it must be noted that it is only valid when the measurements are performed under optimum conditions. It has been experimentally verified that the static noise depends on the sample material and roughness, and it can be optimized by adjusting the frequency and LED parameters. Moreover, the value of 99 nm cannot always be achieved, since the static noise is dependent on the sample's surface.
  - Confocal resolution: The confocal resolution is limited by the transmission of data from the controller to the computer, 15 bits, which results in a resolution of 122 nm (ε_{CS}).
  - Confocal linearity errors: According to the manufacturer, de maximum linearity error is 190 nm (ε_{CS}).
- Piezostage inaccuracies ({0}-{LS}): The nPoint piezostage has been specifically designed for scanning probe and optical microscopy. It has a working range of 100 µm (X) × 100 µm (Y) × 10 µm (Z). Its linearity errors and the value of its noise are given by the manufacturer.
  - The linearity errors are position dependent, with a value of 0.05 % in the XY-plane ($\delta_x^{\{S\}}, \delta_y^{\{S\}}$) and of 0.5 % in the Z-axis ($\delta_z^{\{S\}}$).
  - The positioning noise is 0.5 nm in the XY-plane ($\delta_x^{\{S\}}, \delta_y^{\{S\}}$) and 0.1 nm in Z-axis ($\delta_z^{\{S\}}$).

b) Misalignments:

- Misalignments between fixed base and moving platform ({0}-{1}): Misalignments between fixed base and moving platform occur during the assembly of the components and may be due to many causes, such as the non-parallelism between airbearing surfaces, or the form error of these surfaces. This results in spurious motions in Z-axis and rotations around X and Y-axes when the moving platform displaces around its working range. The spurious motions are measured by the capacitive sensors and corrected in the final measurement.
  - Non-parallelism between capacitive probes and targets: The lack of parallelism between probes and targets results in a positive offset shift in the output, causing the target to appear closer. The manufacturer provides a formula to calculate this error. However, in this case, considering the maximum possible misalignments, the resultant error is smaller than 1 nm, and, therefore, negligible.
  - Repeatability of the compensation of spurious motions in the measurement in Z-axis: The lack of repeatability of the compensation of spurious motions in Z-axis may be caused by numerous error sources such as target surface inaccuracies, deformations of the airbearings' flexures, deformations of the airbearing surfaces, etc. The repeatability has been experimentally measured according to the following procedure: The moving platform trajectory has been programmed to stop along a mesh of points separated 5 mm in X and Y-axes. At these points, the airbearings are turned off and the readouts of the capacitive sensors are recorded. The procedure has been repeated on different days and the results have been analysed. Taken into account the worst results with a uniform distribution, the effective value of the repeatability of the compensation at the centre of the moving platform is 59.04 nm ($\delta_z^{\{1\}}$).
  - Non-orthogonality between laser system and capacitive sensors: The misalignments between the laser system and the capacitive sensors can be known by measuring the non-orthogonality between plane mirrors and capacitive targets with a Coordinate Measuring Machine (CMM) during the assembly phase, and the resultant errors compensated. Consequently, in the uncertainty budget only the uncertainty with which the misalignment is measured is taken into account, that is 1.14×10^{-6} rad for $\alpha_{zx}^{\{1\}}$ and 1.31×10^{-6} rad for $\alpha_{zy}^{\{1\}}$, with a uniform distribution.
- Misalignments between confocal and moving platform ({1}-{CS}): The confocal sensor is fixed to the moving platform before the measuring procedure, and, this assembly results in misalignments. These angles can be obtained by calibration techniques, with an uncertainty that is directly related to the precision of the measuring system. Another option is to measure these angular deviations with a CMM, then, only the uncertainty of the measurement would be taken into account in the uncertainty budget, that is 1×10^{-5} rad for both angles, with a uniform distribution.
- Misalignments between inferior base and levelling system with piezostage {0}-{LS}. As previously stated, the levelling system that contains the piezostage is adjusted before the measuring procedure using the motorized micrometre.
  - Angular deviation between X-axes of the laser system and the piezostage ($\varepsilon_{z,0}^{\{LS\}}$). This angular deviation can be obtained by calibration techniques or measured by the CMM with an uncertainty of 1×10^{-5} rad.
  - Rotation around X and Y-axes $\varepsilon_{x,o}^{\{LS\}}$, $\varepsilon_{y,o}^{\{LS\}}$ of the piezostage. As in the previous case, these angular deviations can be obtained by calibration techniques with an uncertainty that depends on the measuring instrument, or directly measured by an adequate instrument. In this work, it is considered that these angles are obtained with an electronic level (EL), with a resultant uncertainty of $4{\cdot}10^{-5}$ rad.
  - Sensibility of the motorized micrometre: The sensibility of this micrometre is 0.1 μm, and it affects the determination of the final position of the piezostage, resulting in an uncertainty of $5.9{\cdot}10^{-7}$ rad in $\varepsilon_{x,o}^{\{LS\}}$ and $1.26{\cdot}10^{-6}$ rad in $\varepsilon_{y,o}^{\{LS\}}$.

c) Environmental deviations:
- Thermal expansion in Z-axis: The main contributors are the thermal expansion of: the airbearings, the metrology frame, the confocal holder and the confocal sensor itself. The thermal expansion of the NanoPla in Z-axis affects the final measurement of the confocal sensor ({CS}). The effect of the temperature in the confocal sensor has been studied, using the piezostage as sample holder. However, due to the internal complexity of the sensor, compensating this error has not been possible. Therefore, the thermal expansion in Z-axis is considered as an uncertainty, and its value is the maximum observed deviation in the confocal sensor measurement per degree Celsius: 65 nm/ºC (ε_{CS}).
- Thermal expansion of the piezostage: During the scanning process, the thermal deviations in the XY-plane are caused by the expansion of the piezostage ($\delta_x^{\{S\}}$, $\delta_y^{\{S\}}$, $\delta_z^{\{S\}}$). However, according to the manufacturer, the closed-loop range of the system will be unaffected by a small temperature change, so that this error influence has been not considered.

4. Total uncertainty budget calculation using Monte Carlo simulations

Once all uncertainty contributors have been identified and their values and probability distributions characterized, in this section Monte Carlo method is used to propagate the uncertainties in the mathematical error model (Equation (14)) by performing random sampling from probability distributions. In this work, 100,000 iterations are performed in order to obtain a representative set of data. It has been verified that for this number of iterations the results stabilize and have a statistical sense, a higher number of iterations (i.e. 1,000,000) results in a variation in the results of less than 1 nm, thus, a higher number of iterations is not necessary.

4.1. Input of the Monte Carlo simulation

Table 1 and Table 2 show the uncertainty contributors during the positioning and the scanning process, respectively, which are taken into account in the Monte Carlo simulations. In the tables, apart from the value of each contributor (previously justified in section 3.2), it is also detailed how the uncertainty estimation has been obtained: the value can be given by the manufacturer (M), obtained by experimental measurements (E), or from scientific literature and references (R). The tables also show the probability distribution (PD) of the uncertainty contributor, and its standard deviation. The standard deviation is calculated directly from the Monte Carlo simulation output set of data.

4.2. Resultant measuring uncertainty along the NanoPla working range

As it can be seen in Equations 15 and 16, the final uncertainty in the measurement is position-dependent, thus, the simulation must be performed for different points in the XY coordinates ($x^{\{1\}}$, $y^{\{1\}}$) that cover the working range of the moving platform (±25 mm, ±25 mm) and the XYZ coordinates ($x^{\{s\}}$, $y^{\{s\}}$, $z^{\{s\}}$) that cover the working range of the piezostage (±50 μm, ±50 μm, ±10 μm).

At each position, the Monte Carlo simulation provides a dataset of n = 100,000 results for the final value of the uncertainty of the measurement in XYZ-coordinates. Fig. 6a shows the dataset obtained for the measuring uncertainty at the border of the NanoPla working range,

Table 1
Uncertainty contributors of the positioning process.

Error type	Source and parts	Description	Component	Value	Method	PD	Standard deviation
Components inaccuracies	Laser system {0}-{1}	Wavelength instability	$\delta_x^{\{1\}}=\delta_y^{\{1\}}$ $\varepsilon_z^{\{1\}}$	<50 ppb	M	Uniform	0.7 nm 1.9×10^{-8} rad
		Sensor resolution	$\delta_x^{\{1\}}=\delta_y^{\{1\}}$ $\varepsilon_z^{\{1\}}$	1.58 nm	M	Uniform	0.5 nm 1.2×10^{-8} rad
		Laser beam mixing	$\delta_x^{\{1\}}=\delta_y^{\{1\}}$ $\varepsilon_z^{\{1\}}$	<2 nm	M	Uniform	1.2 nm 4.2×10^{-8} rad
		RMSD	$\delta_x^{\{1\}}=\delta_y^{\{1\}}$ $\varepsilon_z^{\{1\}}$	5.4 nm	E [36]	Normal	5.4 nm 1.97×10^{-7} rad
System misalignments	Laser system {0}-{1}	Plane mirror form errors	$\delta_x^{\{1\}}=\delta_y^{\{1\}}$ $\varepsilon_z^{\{1\}}$	633/10 nm per 100 mm	M	Uniform	15.8 nm 5.72×10^{-7} rad
		Misalignment between laser beam and plane mirror	$\delta_x^{\{1\}}=\delta_y^{\{1\}}$ $\varepsilon_z^{\{1\}}$	$\ll$ 1 nm	M	Negligible	
		Misalignment between laser beams and plane of motion	$\delta_x^{\{1\}}=\delta_y^{\{1\}}$ $\varepsilon_z^{\{1\}}$	<25 nm	R [37]	Uniform	14.4 nm 3.71×10^{-7} rad
		Non-squareness between laser beams	$\alpha_{xy}^{\{1\}}$	1×10^{-6} rad	R [37]	Uniform	5.77×10^{-7} rad
Environmental deviations	Laser system {0}-{1}	Refractive index environmental compensation	$\delta_x^{\{1\}}=\delta_y^{\{1\}}$ $\varepsilon_z^{\{1\}}$	1 ppm	M	Uniform	2.5 nm 6.4×10^{-8} rad
	Metrology frame {0}-{1}	Thermal expansion	$\delta_x^{\{1\}}\delta_y^{\{1\}}\varepsilon_z^{\{1\}}$	19 nm 24 nm	E [36]	Normal	19 nm 24 nm 4.35×10^{-7} rad

when the moving platform nominal position is $x^{\{1\}} = 0$ mm, $y^{\{1\}} = 25$ mm, the piezostage nominal position is $x^{\{s\}} = 50\ \mu$m, $y^{\{s\}} = 50\ \mu$m, $z^{\{s\}} = 5\ \mu$m, the confocal sensor readout, z_{CS}^{exp}, has been set equal to 2 mm, and its position offset, z_o^{CS}, equal to 0 mm. At this position, the expanded uncertainty that provides an interval with 95 percent of the resultant values of the Monte Carlo simulation are the following at X, Y and Z-axes respectively: $U_{95,x} = 247.24$ nm, $U_{95,y} = 93.26$ nm, $U_{95,z} = 944.22$ nm.

In addition, to study how the measuring uncertainty varies along the working range of the NanoPla, Monte Carlo simulations have been performed along different points covering the area. Fig. 6b shows the measuring uncertainty along one quadrant of the working range, since the results are symmetric with respect to X and Y-axes. These measuring uncertainties (u_x, u_y, u_z) have been calculated as the standard deviation of the 100,000 results obtained for each position (k = 1). In all the cases, the piezostage nominal position is $x^{\{s\}} = 50\ \mu$m, $y^{\{s\}} = 50\ \mu$m, $z^{\{s\}} = 5\ \mu$m, to consider the highest possible contribution. In addition, the confocal sensor readout, z_{CS}^{exp}, has been set equal to 2 mm, and its position offset, z_o^{CS}, equal to 0 mm.

As shown in Fig. 6b, the measuring uncertainty in Z-axis is the highest along the whole working range, being 169.81 nm at the position X = 0.05 mm, Y = 0.05 mm, Z = 0.005 mm. This is due to the fact that the confocal sensor measuring errors are one of the highest contributors. In addition, as shown in Equation 16, the angular deviations of the levelling system and the piezostage around X and Y-axes ($\varepsilon_{x,o}^{LS}$, $\varepsilon_{y,o}^{LS}$) contribute to the measuring uncertainty in Z-axis, multiplied by the displacement of the moving platform in X and Y-axes ($x^{\{1\}}$, $y^{\{1\}}$), thus, it increases when the moving platform displaces from the reference position (0,0), being 836.19 nm at the position X = 25.05 mm, Y = 25.05 mm, Z = 0.005 mm.

Similarly, the uncertainty in X-axis increases when the platform displaces along Y-axis, and the uncertainty in Y-axis increases when the platform displaces in X-axis. Fig. 6b shows that the measuring uncertainty in X and Y-axes at the position X = 0.05 mm, Y = 0.05 mm is u_x = 57.72 nm and u_y = 57.40 nm, respectively; the measuring uncertainty at the position X = 12.55 mm, Y = 12.55 mm is u_x = 92.36 nm and u_y = 92.13 nm, while the measuring uncertainty at the position X = 25.05 mm, Y = 25.05 mm is u_x = 154.70 nm and u_y = 155.08 nm. However, considering relative uncertainties, at the position X = 12.55 mm, Y = 12.55 mm, the relative uncertainty in X and Y-axes are u_x/x = 7.34 nm/mm and u_y/y = 7.34 nm/mm, while at the position X = 25.05 mm, Y = 25.05 mm, the relative uncertainties are u_x/x = 6.18 nm/mm and u_y/y = 6.19 nm/mm. This is due to the fact that one of the contributors in X and Y-axes is the angular deviation of the piezostage ($\varepsilon_{z,o}^{LS}$) multiplied by the displacement of the moving platform in Y-axis in the case of the X-axis measuring uncertainty, and by the displacement in X-axis, in the case of the Y-axis measuring uncertainty. Therefore, in the three axes, the measuring uncertainty is magnified when the moving platform is displaced from the reference position (0,0).

On the other hand, in order to study the influence of the piezostage positioning uncertainty, the measuring uncertainty has been calculated along different points of its working range in the XY-plane, and for $z^{\{s\}} = 5\ \mu$m. The moving platform is considered to be at the reference position (0,0), in order to cancel the errors associated to its displacement. Similarly, due to the fact that the errors of the confocal sensor are much higher than the piezostage errors, they have been eliminated in this calculation, considering that the NanoPla could integrate more precise instruments. The capacitive sensor system, as well as the laser system are part of the NanoPla and are not exchangeable, thus, their influence has been maintained. Fig. 7a shows the dataset obtained for the measuring uncertainty at the border of the piezostage working range, when its nominal position is $x^{\{S\}} = 0\ \mu$m, $y^{\{S\}} = 50\ \mu$m and $z^{\{S\}} = 5\ \mu$m. At this position, the expanded uncertainty that provides an interval with 95 percent of the resultant values of the Monte Carlo simulation are the following at X, Y and Z-axes respectively: $U_{95,x} = 48.19$ nm, $U_{95,y} = 52.88$ nm, $U_{95,z} = 139.33$ nm. The error map is shown in Fig. 7b. As seen, the measuring uncertainty in X and Y-axes increases when the piezostage displaces from its reference position (0,0), this is due to the fact that the uncertainty of the angular deviations of the piezostage ($\varepsilon_{x,o}^{LS}$, $\varepsilon_{y,o}^{LS}$, $\varepsilon_{z,o}^{LS}$) are multiplied by the displacement. However, since the piezostage displaces in a small range, the variation of the measuring uncertainty is minimal. The main uncertainty contributors in X and Y-axes are the laser system measuring errors, the thermal expansion of the metrology frame and the linearity errors of the piezostage. In Z-axis, one of the main contributors to the measuring uncertainty are the measuring errors and repeatability of the capacitive sensors system, which is independent on the displacement.

Table 2
Uncertainty contributors of the scanning process.

Error type	Source and parts	Description	Compo-nent	Value	Method	PD	Standard deviation
Components' inaccuracies	Capacitive sensors {0}-{1}	RMSD	$\delta_z^{\{1\}}\varepsilon_x^{\{1\}}\varepsilon_y^{\{1\}}$	C1 = C2 = C3 = 57.08 nm	E [38]	Uniform	34.2 nm [2] 2.58×10^{-7} rad 2.42×10^{-7} rad
		Positioning error	$\delta_z^{\{1\}}\varepsilon_x^{\{1\}}\varepsilon_y^{\{1\}}$	C1 = 28 nm C2 = 202 nm C3 = 164 nm	M	Uniform	60.80 nm [2] 2.84×10^{-7} rad 3.52×10^{-7} rad
	Confocal sensor {CS}	Static Noise	ε_{sc}	99 nm	E, M	Normal	99 nm
		Resolution	ε_{sc}	122 nm	E, M	Uniform	70.4 nm
		Linearity errors	ε_{sc}	190	M	Uniform	109.7 nm
	Piezo stage {LS}-{S}	Linearity errors	$\delta_x^{\{S\}}=\delta_y^{\{S\}}$ $\delta_z^{\{S\}}$	0.05 % 0.5 %	M	Uniform	14.4 nm [1] 1.4 nm [1]
		Positioning noise	$\delta_x^{\{S\}}=\delta_y^{\{S\}}$ $\delta_z^{\{S\}}$	0.5 nm 0.1 nm	M	Uniform	0.5 nm 0.1 nm
	Motorized micro-metre {LS}-{S}	Sensibility	$\varepsilon_{x,o}^{\{LS\}}\varepsilon_{y,o}^{\{LS\}}$	$5.9{\cdot}10^{-7}$ rad $1.26{\cdot}10^{-6}$ rad	M	Uniform	3.41×10^{-7} rad 7.26×10^{-7} rad
System Misalignments	Capacitive sensors and targets {0}-{1}	Non-parallelism between probes and targets	$\delta_z^{\{1\}}\varepsilon_x^{\{1\}}\varepsilon_y^{\{1\}}$	$\ll 1$ nm	M, R	Negligible	
		Repeatability of the compensation	$\delta_z^{\{1\}}\varepsilon_x^{\{1\}}\varepsilon_y^{\{1\}}$	C1 = C2 = C3 = 171 nm	E	Uniform	59.1 nm [2] 4.48×10^{-7} rad 4.18×10^{-7} rad
		Non-orthogonality between laser system and capacitive sensors	$\alpha_{zx}^{\{1\}}\alpha_{yz}^{\{1\}}$	1.14×10^{-6} rad 1.31×10^{-6} rad	E (CMM)	Uniform	1.14×10^{-6} rad 1.31×10^{-6} rad
	Confocal sensor and moving platform {1}- {CS}	Angular deviation of the sensor Z-axis	$\varepsilon_x^{\{CS\}} = \varepsilon_y^{\{CS\}}$	1×10^{-5} rad	E (CMM)	Uniform	5.78×10^{-6} rad
	Levelling system and fixed base {0}- {LS}	Angular deviation of the piezostage	$\varepsilon_x^{\{LS\}} = \varepsilon_y^{\{LS\}}\varepsilon_z^{\{LS\}}$	4×10^{-5} rad 1×10^{-5} rad	E (EL) E (CMM)	Uniform	2.31×10^{-5} rad 5.78×10^{-6} rad
Environmental deviations	Thermal expansions {CS}	Thermal expansion confocal sensor {CS}	ε_{sc}	65 nm/°C	E (external setup)	Weibull	39.44 nm
	{0}-{LS}	Thermal expansions piezostage {0}-{LS}	$\delta_x^{\{S\}}=\delta_y^{\{S\}}$ $\delta_z^{\{S\}}$	$\ll 1$ nm	M	Negligible	

[1] Position dependent. Value shown for the position X = 50 μm; Y = 50 μm; Z = 5 μm of the piezostage (worst case scenario).
[2] Effective value at the center of the moving platform. Position dependent, value shown for the position X = 25 mm; Y = 25 mm (worst case scenario).

4.3. Influence of the NanoPla different contributors in the final measuring uncertainty

In order to study the individual contribution of the different components of the NanoPla, Monte Carlo simulations have been performed considering their influence separately. The contributors have been divided by components: laser system, capacitive sensors, confocal sensor, piezostage and motorized micrometer. Moreover, all the misalignments in the assembly are also considered as a unique contributor, since they can be reduced during the assembly and evaluated by calibration methods. Similarly, thermal expansion is also considered as a unique contributor, since it can be reduced by improving the temperature control. However, laser system refractive index environmental compensation and plane mirror form errors are considered inside the laser system contribution, since they are intrinsic to the laser system. Table 3 shows the results for the moving platform at the reference position ($x^{\{1\}} = 0, y^{\{1\}} = 0$), and at the edge of its working range ($x^{\{1\}} = 25, y^{\{1\}} = 25$). In all the cases, the piezostage nominal position is $x^{\{s\}} = 50\,\mu$m, $y^{\{s\}} = 50\,\mu$m, $z^{\{s\}} = 5\,\mu$m, to consider the highest possible contribution. In addition, the confocal sensor readout, z_{CS}^{exp}, has been set equal to 2 mm, and its position offset, z_o^{CS}, equal to 0 mm. It can be observed that, at the reference position, the highest contributor in X and Y-axes are the misalignments in the assembly, followed by the thermal expansion, while the highest contributor in Z-axis is the confocal sensor, followed by the misalignments in the assembly. Similarly, at the edge of the NanoPla working range, the highest contributors in the three axes are the misalignments in the assembly, which are the only errors whose influence is highly amplified when the moving platform displaces from the reference position.

In addition, from Equations 15 and 16, it can be inferred that the magnitude of the confocal sensor readout (z_{CS}^{exp}) affects the final measurement uncertainty, which have a maximum range of 4 mm (±2 mm). Similarly, the position of the confocal sensor in Z-axis (z_o^{CS}) also affects the final measurement uncertainty.

The influence of the magnitude of the position of the confocal sensor, z_o^{CS}, and the magnitude of its readout, z_{CS}^{exp}, are following studied at the reference position of the moving platform (0,0), to cancel the errors caused by its displacement, none of the other uncertainty contributors has been cancelled in this calculation. The results are shown in Table 4.

It can be inferred from Table 4 that the position of the confocal

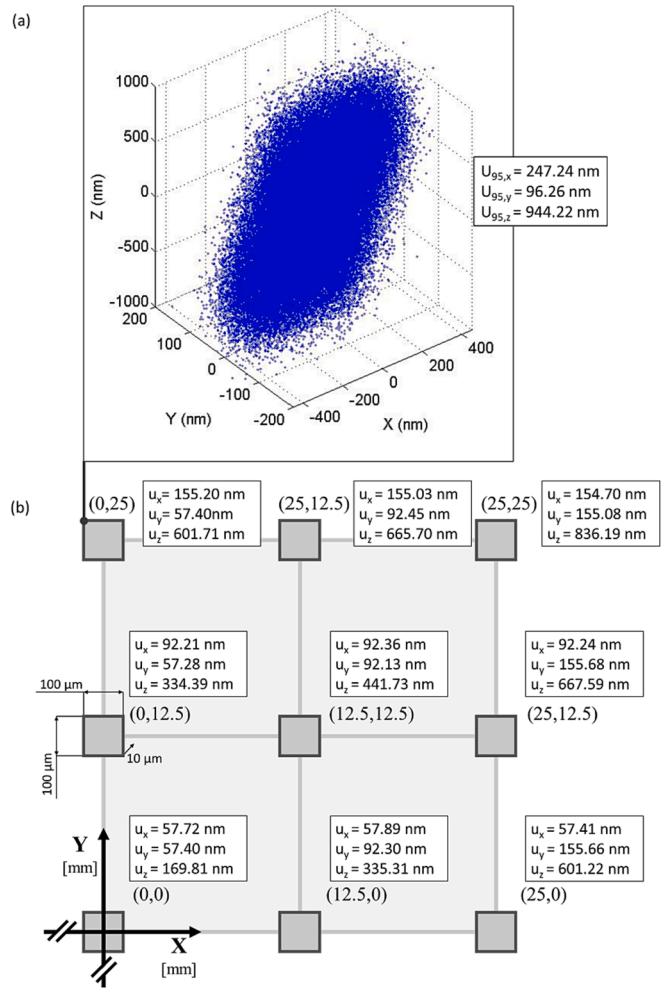

Fig. 6. (**a**) Scatter diagram of the final uncertainty in n = 100,000 measurements, at the position X = 0.05 mm, Y = 25.05 mm and Z = 0.005 mm. (**b**) Measuring uncertainty map along the working range of the NanoPla.

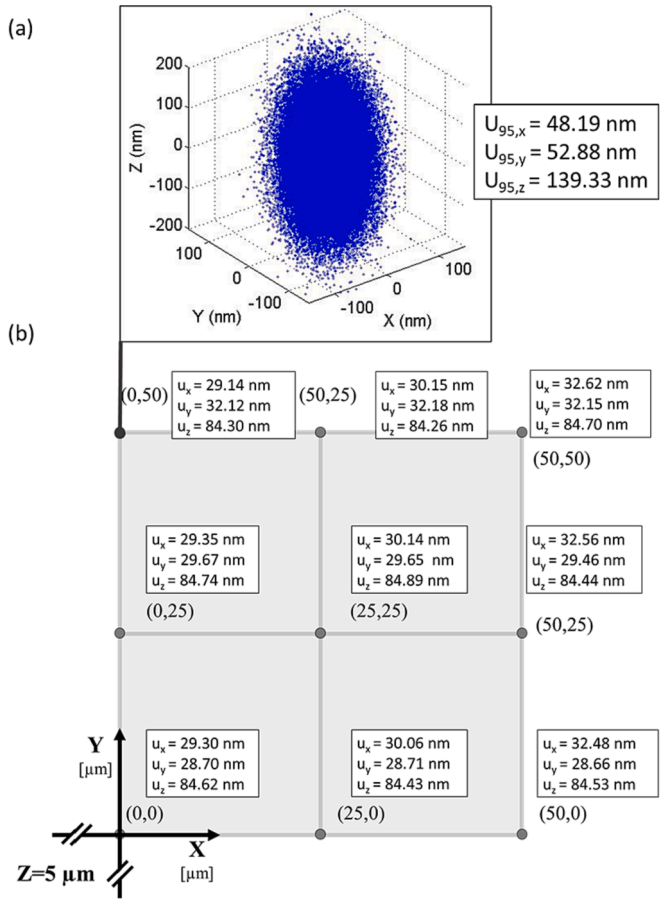

Fig. 7. (**a**) Scatter diagram of the final uncertainty in n = 100,000 measurements, at the position X = 0 mm, Y = 0.05 mm and Z = 0.005 mm. (**b**) Measuring uncertainty map along the working range of the piezostage, with the moving platform at the reference position (0,0).

sensor in the moving platform has a great influence in the final measuring uncertainty in X and Y-axes. Equation (15) shows that this is because in X-axis, z_o^{CS} is directly multiplied by the angular deviations $\varepsilon_{y,o}^{\{LS\}}$, $\varepsilon_y^{\{1\}}$, being $\varepsilon_{y,o}^{\{LS\}}$ the most significant. The term z_o^{CS} is also included in the calculation of Z-axis measuring uncertainty (Equation 16), but, in this case, it is multiplied by angular deviations that are, in turn, multiplied between themselves, reducing their effect. That is why, the Z-axis measuring uncertainty seems unaffected by the variation of z_o^{CS}.

It can also be inferred from Table 4 that, when the magnitude of the confocal sensor readout increases, the measuring uncertainty also increases significantly in X and Y-axes. As shown in Equation (15), this is due to the fact that, in the case of X-axis, the value z_{CS}^{exp}, is directly multiplied by the angular deviations $\varepsilon_{y,o}^{LS}$, $\varepsilon_{y,o}^{CS}$ and $\varepsilon_y^{\{1\}}$, being $\varepsilon_{y,o}^{LS}$ the most significant (Table 2). The measuring uncertainty in Z-axis seems to be unaffected by the variations of z_{CS}^{exp}, that is because, although, z_{CS}^{exp} is also multiplied by angular deviations in the calculation of Z-axis measuring uncertainty (Equation 16), they are also multiplied between themselves, reducing their effective value.

4.4. Good practices inferred from the Monte Carlo simulations

In this section, it has been analyzed how the position of the NanoPla affects its final uncertainty. The displacement of the moving platform along its working range (±25 mm, ±25 mm) has a great effect in the three coordinates of the measuring uncertainty, due to the fact that the angular errors are amplified by the distance, being the main uncertainty contributor when displacing from the reference position (0,0). In contrast, the short-range displacement of the piezostage along its working range (±50 µm, ±50 µm) has an insignificant influence in the final uncertainty. Therefore, in order to minimize the errors caused by the moving platform displacement, the sample should be placed centered in the NanoPla working range, by matching, when possible, the center of the sample with the NanoPla reference position (0,0). In this manner, the displacements from the reference position will be minimized, and, hence, the measuring uncertainty. Moreover, it has been observed that the uncertainties in the determination of the angular deviations of the levelling system and piezostage ($\varepsilon_{x,o}^{LS}$, $\varepsilon_{y,o}^{LS}$, $\varepsilon_{z,o}^{LS}$) are the highest contributors, thus, they should be minimized by using more precise instruments for their determination, or by defining calibration procedures.

On the other hand, Monte Carlo simulations prove that the confocal sensor position and its readouts also have a significant effect in the final measuring uncertainty. The smallest uncertainties are achieved when the offset of the confocal sensor origin (z_o^{CS}) is equal to zero, that is when the reference readout of the confocal sensor is coincident with the point at which the XY-plane of the laser system intersects with the confocal sensor beam (Fig. 8). It must be noted that in order to do that, the measured surface must also intersect with the laser system XY-plane. In addition, when possible, the whole measuring surface of the sample should be contained inside the working range of the confocal sensor.

Finally, the magnitude of the confocal sensor readouts also

Table 3
Contribution to the measuring uncertainty of the NanoPla components.

$x^{\{1\}}, y^{\{1\}}$	Contributor	u_x [nm]	u_x [%]	u_y [nm]	u_y [%]	u_z [nm]	u_z [%]
0 mm,	Laser system	16.84	8.56 %	11.91	4.30 %	0	0.00 %
0 mm	Capacitive sensors	0.86	0.02 %	0.77	0.02 %	60.83	12.80 %
	Confocal sensor	11.56	4.04 %	11.54	4.03 %	142.11	69.88 %
	Piezostage	14.46	6.31 %	14.49	6.36 %	14.44	0.72 %
	Motorized micrometre	1.45	0.06 %	0.68	0.01 %	0.04	0.00 %
	Misalignments in the assembly	48.17	70.07 %	47.30	67.76 %	57.06	11.27 %
	Thermal expansion	19.02	10.93 %	24.05	17.52 %	39.23	5.33 %
	Total	**57.72**	**100 %**	**57.40**	**100 %**	**169.81**	**100 %**
25 mm,	Laser system	16.88	1.18 %	11.92	0.59 %	0	0.00 %
25 mm	Capacitive sensors	0.86	0.00 %	0.77	0.00 %	69.89	0.70 %
	Confocal sensor	11.56	0.55 %	11.54	0.55 %	142.40	2.92 %
	Piezostage	14.46	0.87 %	14.49	0.87 %	14.44	0.03 %
	Motorized micrometre	1.45	0.01 %	0.68	0.00 %	20.06	0.06 %
	Misalignments in the assembly	152.06	95.88 %	152.34	95.63 %	816.65	96.06 %
	Thermal expansion	19.05	1.50 %	23.95	2.36 %	39.46	0.22 %
	Total	**154.70**	**100 %**	**155.08**	**100 %**	**836.19**	**100 %**

Table 4
Measuring uncertainty of the NanoPla for different values of z_o^{CS} and z_{CS}^{exp}.

z_o^{CS} [mm]	z_{CS}^{exp} [mm]	$x^{\{1\}}$, $y^{\{1\}}$	$x^{\{s\}}, y^{\{s\}}$, $z^{\{s\}}$	u_x [nm]	u_y [nm]	u_z [nm]
20	0	0, 0	0, 0, 0	463.36	462.89	170.31
10	0	0, 0	0, 0, 0	233.11	232.60	169.67
1	0	0, 0	0, 0, 0	37.32	36.83	169.54
0	0	0, 0	0, 0, 0	29.17	28.67	169.67
0	1	0, 0	0, 0, 0	37.65	37.28	169.41
0	2	0, 0	0, 0, 0	55.90	55.36	169.30
0	4	0, 0	0, 0, 0	99.71	99.35	169.40

influences the final measuring uncertainty. In order to minimize the maximum measured value, the reference of the confocal sensor readouts should be taken at a point of the sample surface that is neither a valley, nor a peak. As it is shown in Table 4, an offset as small as 1 mm in any of these two values, increases around 28 % the measuring uncertainty in X and Y-axes, so it is important to standardize this process in order to minimize possible deviations caused by the human factor. Fig. 8 shows a correct positioning of the sample and the confocal sensor. As it can be seen, the sample surface is contained in the 4-mm working range of the confocal sensor. The reference of the confocal sensor readouts is taken at the point of the sample surface at which the sensor beam intersects with the laser system XY-plane. In order to achieve that, it may be necessary to use auxiliary elements to take the reference readout of the confocal sensor, and to elevate the sample to the right level, before the measurement.

5. Conclusions

This work presents a procedure for performing an uncertainty budget in order to estimate the final measuring uncertainty of a precision metrology system after error compensation, using Monte Carlo simulations. This procedure is implemented in the NanoPla, a 2D-long range nanopositioning stage, with a confocal sensor integrated. During the design of the NanoPla, in previous works, precision system design principles, such as error budget, have been applied. Once the NanoPla is a functional system, its errors have been characterized and compensated when possible. Therefore, in this work, when the errors are compensated, only the uncertainty of that compensation affects the final measurement, and, thus, the final measuring uncertainty.

The first step of the uncertainty budget procedure is knowing the structure, the parts and the components of the system, as well as its measuring procedure. In the specific case of the NanoPla, the measuring procedure consists in a positioning process, and, in a scanning process, which are performed separately and consecutively. Then, the mathematical error model needs to be obtained. For that purpose, it is important to define a coordinate reference system for each part, and identify all the relative movements between them. Once this is done, the uncertainty budget contributors must be identified, characterized and located in the transformation matrixes and vectors of the mathematical error model. The uncertainty budget contributors are divided into two groups, depending on whether they occur during the positioning process or during the scanning process. Inside these groups, they are divided into three subgroups, depending on their cause: component inaccuracies, misalignments between parts and environmental deviations. Then,

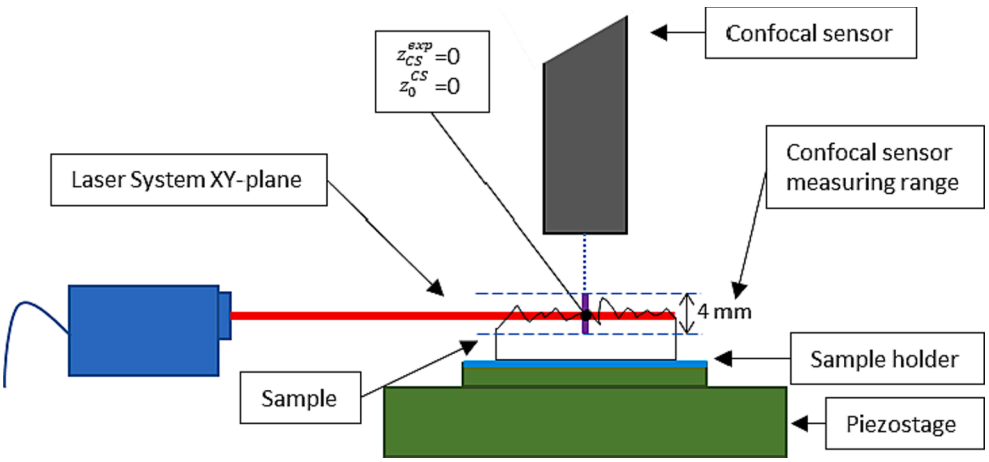

Fig. 8. Scheme of the confocal sensor position with respect to the Laser system XY-plane and the sample.

Monte Carlo method is used to propagate the uncertainties in the mathematical error model, and to obtain the final measuring uncertainty of the NanoPla along its working range, considering all the casuistry, such as different positions of the confocal sensor. The results show that the measuring uncertainty is position dependent, and, it increases when the moving platform displaces further from its reference position (0,0). In addition, the confocal sensor position in Z-axis in the moving platform, which depends on the sample surface height, is also a relevant uncertainty contributor. After analyzing the results, good practices during the measuring procedure are proposed to minimize the final measuring uncertainty.

Using the NanoPla as a case study, our work provides a methodology that is totally reproducible in any precision system, being this a remarkable scientific contribution. For that reason, the transformation matrices and vectors of the mathematical model are defined thoroughly, being this part one of the most crucial for the correct calculation of the uncertainty budget. Another crucial part is the uncertainty contributors' identification. In this work, authors also define each of them for the NanoPla case as a way to help reproducibility of this analysis in different works with other precision systems, whose uncertainty contributors will probably be similar. It must be highlighted that the uncertainty budget presented in this work is performed on a functional system and, thus, the contributors to the measuring errors can be directly measured and compensated when possible. For this reason, it is important to define how they are measured to estimate the uncertainty of their compensation. In addition, although in a functional system is not possible to make changes in the structural design anymore, the uncertainty budget allows optimizing the operating procedure to minimize some of the uncertainty contributions.

In this article, the measuring scanning process is considered independent from the positioning process. Nevertheless, the NanoPla is also capable of measuring while performing motion. In this type of measurement, more error contributors are involved, such as dynamic errors. For that case, a new uncertainty budget should be performed. In this line, future work should focus on defining calibrations procedures to reduce the uncertainty of the compensation of angular deviations of the piezostage, which are the greatest contributors when the NanoPla displaces from its reference position.

Funding

This research was funded by the Ministerio de Ciencia e Innovación (MCI) of the Spanish government, the Agencia Estatal de Investigación (AEI) of Spain, and the Fondo Europeo de Desarrollo Regional (FEDER), project RTI2018-097191-B-I00 "MultiMet"; and by Gobierno de Aragón (Ref. Group T56_20R) and co-funded with Feder 2014–2020 "Construyendo Europa desde Aragón".

CRediT authorship contribution statement

L.C. Díaz-Pérez: Conceptualization, Methodology, Software, Validation, Formal analysis, Investigation, Writing – original draft, Writing – review & editing. **M. Torralba:** Conceptualization, Methodology, Software, Validation, Formal analysis, Investigation, Writing – review & editing. **L. Muro:** Validation, Formal analysis, Investigation. **J.A. Albajez:** Conceptualization, Methodology, Software, Writing – review & editing. **J.A. Yagüe-Fabra:** Conceptualization, Methodology, Software, Writing – review & editing.

Declaration of Competing Interest

The authors declare that they have no known competing financial interests or personal relationships that could have appeared to influence the work reported in this paper.

Data availability

Data will be made available on request.

References

[1] V.C. Venkatesh, S. Izman, Precision Engineering, McGraw-Hill, 2017.
[2] P.A. McKeown, The Role of Precision Engineering in Manufacturing of the Future, CIRP Ann. 36 (2) (1987) 495–501.
[3] E.G.G. Loewen, Metrology Problems in General Engineering: A Comparison with Precision Engineering, CIRP Ann. 29 (2) (Feb. 1980) 451–453.
[4] L.C. Hale, Principles and techniques for design precision machines. PhD Thesis, University of California, 1999.
[5] P.A. Mckeown, High Precision Manufacturing and the British Economy, Proc. Inst. Mech. Eng. Part B J. Eng. Manuf. 200 (3) (1986) 147–165.
[6] P. Schellekens, N. Rosielle, H. Vermeulen, M. Vermeulen, S. Wetzels, W. Pril, Design for Precision: Current Status and Trends, CIRP Ann. - Manuf. Technol. 47 (2) (1998) 557–586.
[7] S. Leach, R. Smith, *Basics of Precision Engineering*, CRC Press, Taylor & Francis Group, Boca Rato, 2018.
[8] E. C. Teague and C. Evans, Patterns for Precision Instrument Design (Mechanical Aspects), in: *NIST Tutorial Notes, ASPE Annual Meeting*, 1989.
[9] J.A. Yagüe-Fabra, W. Gao, A. Archenti, E. Morse, A. Donmez, Scalability of precision design principles for machines and instruments, CIRP Ann. 70 (2021).
[10] H. Haitjema, Measurement Uncertainty, in: L. Laperrière, G. Reinhart (Eds.), CIRP Encyclopedia of Production Engineering, Springer, Berlin Heidelberg, Berlin, 2014, pp. 852–857.
[11] W. Tian, W. Gao, D. Zhang, T. Huang, A general approach for error modeling of machine tools, Int. J. Mach. Tools Manuf. 79 (2014) 17–23.
[12] W. Zhu, Z. Wang, K. Yamazaki, Machine tool component error extraction and error compensation by incorporating statistical analysis, Int. J. Mach. Tools Manuf. 50 (9) (2010) 798–806.
[13] L. Andolfatto, J.R.R. Mayer, S. Lavernhe, Adaptive Monte Carlo applied to uncertainty estimation in five axis machine tool link errors identification with thermal disturbance, Int. J. Mach. Tools Manuf. 51 (7–8) (2011) 618–627.
[14] E. Creighton, A. Honegger, A. Tulsian, D. Mukhopadhyay, Analysis of thermal errors in a high-speed micro-milling spindle, Int. J. Mach. Tools Manuf. 50 (4) (2010) 386–393.
[15] S.H. Chang, C.K. Tseng, H.C. Chien, An ultra-precision XY/spl theta//sub Z/ piezo-micropositioner. I. Design and analysis, IEEE Trans. Ultrason. Ferroelectr. Freq. Control 46 (4) (1999) 897–905.
[16] J. Gouws, Error budgeting for control system design, R&D J. 11 (3) (1995) 61–67.
[17] A.H. Slocum, Precision machine design, Prentice-Hall, 1992.
[18] S. Postnikov, S. Hector, C. Garza, R. Peters, V. Ivin, Critical dimension control in optical lithography, Microelectron. Eng. 69 (2–4) (2003) 452–458.
[19] J. Eguia, A. Lamikiz, L. Uriarte, Error budget and uncertainty analysis of portable machines by mixed experimental and virtual techniques, Precis. Eng. 47 (2017) 19–32.
[20] Y. Sun, W. Chen, Y. Liang, C. An, G. Chen, H. Su, Dynamic error budget analysis of an ultraprecision flycutting machine tool, Int. J. Adv. Manuf. Technol. 76 (5–8) (2014) 1215–1224.
[21] L. Uriarte, et al., Error budget and stiffness chain assessment in a micromilling machine equipped with tools less than 0.3 mm in diameter, Precis. Eng. 31 (1) (2007) 1–12.
[22] J. Walter, M.M. Norlund, B. Koning, R.J. Roblee, Error budget as a design tool for ultra-precision diamond turning machines, in *Proceedings of the ASPE's 17th Annual Meeting*, 2002.
[23] P. Soons, J.A. Theuws, F.C. Schellekens, Modelling the errors of multi-axis machines: a general methodology, Precis. Eng. 14 (1) (1992) 5–19.
[24] E. Treib, T. Matthias, Error budgeting—applied to the calculation and optimization of the volumetric error field of multiaxis systems, Ann. CIRP 36 (1) (1987) 365–368.
[25] Y. Liu, M. Yuan, J. Cao, J. Cui, J. Tan, Evaluation of measurement uncertainty in H-drive stage during high acceleration based on Monte Carlo method, Int. J. Mach. Tools Manuf. 93 (2015) 1–9.
[26] R.C. Kochanski, Systematic approach to error budget analysis for integrated sensor systems, AIAA/IEEE Digit. Avion. Syst. Conf. - Proc. 1 (2002) 1–10.
[27] U. Mutilba, G. Kortaberria, F. Egaña, J. A. Yagüe-Fabra, Relative pointing error verification of the telescope mount assembly subsystem for the large synoptic survey telescope, in: *5th IEEE Int. Work. Metrol. AeroSpace, Metroaerosp. 2018 - Proc.*, 2018, pp. 155–160.
[28] A.J. Hart, A. Slocum, P. Willoughby, Kinematic coupling interchangeability, Precis. Eng. 28 (1) (2004) 1–15.
[29] M. Torralba, M. Valenzuela, J.A. Yagüe-Fabra, J.A. Albajez, J.J. Aguilar, Large range nanopositioning stage design: A three-layer and two-stage platform, Meas. J. Int. Meas. Confed. 89 (2016) 55–71.
[30] M. Torralba, J.A. Yagüe-Fabra, J.A. Albajez, J.J. Aguilar, Design optimization for the measurement accuracy improvement of a large range nanopositioning stage, Sensors 16 (1) (2016) pp.
[31] E. Manske, G. Jäger, T. Hausotte, R. Füßl, Recent developments and challenges of nanopositioning and nanomeasuring technology, Meas. Sci. Technol. 23 (7) (Jul. 2012), 074001.
[32] H.-J. Büchner, G. Jäger, A novel plane mirror interferometer without using corner cube reflectors, Meas. Sci. Technol. 17 (4) (2006) 746–752.

[33] H. Schwenke, W. Knapp, H. Haitjema, A. Weckenmann, R. Schmitt, F. Delbressine, Geometric Error Measurement and Compensation of Machines - An update, CIRP Ann. 57 (2) (2008) 660–675.
[34] J.A. Kim, J.W. Kim, C.-S. Kang, T.B. Eom, Metrological atomic force microscope using a large range scanning dual stage, Int. J. Precis. Eng. Manuf. 10 (5) (2009) 11–17.
[35] L. Díaz-Pérez, M. Torralba, J.A. Albajez, J.A. Yagüe-Fabra, 2D Positioning Control System for the Planar Motion of a Nanopositioning Platform, Procedia Manuf. 41 (2019) 249–256.
[36] L. Díaz-Pérez, M. Torralba, J. A. Albajez, J. A. Yagüe, Performance analysis of laser measuring system for an ultra-precision 2D-stage, in: *euspen's 17th International Conference & Exhibition*, 2017, pp. 66–67.
[37] M. Torralba, L.C. Díaz-Pérez, M. Valenzuela, J.A. Albajez, J.A. Yagüe-Fabra, Geometrical characterisation of a 2D laser system and calibration of a cross-grid encoder by means of a self-calibration methodology, Sensors (Switzerland) 17 (9) (2017) pp.
[38] L. Díaz-Pérez, M. Torralba, J. A. Albajez, J. A. Yagüe, Study of Z-direction performance of a XY nanopositioning stage, in: *Euspen's Virtual International Conference*, 2020, pp. 231–232.